A Power-Efficient Oscillatory Synchronization Feature Extractor for Closed-Loop Neuromodulation

Yassin, Hoda; Akhoundi, Arash ; Hasaneen, El Sayed; Muratore, Dante

DOI
10.1109/TCSII.2024.3353927

Publication date
2024

Document Version
Final published version

Published in
IEEE Transactions on Circuits and Systems II: Express Briefs

Citation (APA)
Yassin, H., Akhoundi, A., Hasaneen, E. S., & Muratore, D. (2024). A Power-Efficient Oscillatory Synchronization Feature Extractor for Closed-Loop Neuromodulation. *IEEE Transactions on Circuits and Systems II: Express Briefs*, *71*(6), 3176-3180. https://doi.org/10.1109/TCSII.2024.3353927

A Power-Efficient Oscillatory Synchronization Feature Extractor for Closed-Loop Neuromodulation

Hoda Yassin, Arash Akhoundi, El-Sayed Hasaneen, and Dante G. Muratore, *Senior Member, IEEE*

***Abstract*—This brief presents a low-power oscillatory synchronization feature extraction (FE) unit for phase-amplitude coupling (PAC) and phase locking value (PLV) features. The proposed FE unit uses a new multiplier-less wavelet approximation in combination with a multi-rate lowpass filter bank for low-power complex signal extraction. Further power and area reductions are obtained by utilizing a light sine and cosine extractor (LSCE) for the feature computation. The synthesized 32-channel design achieves state-of-the-art performances in post-layout simulations at 430 nW/channel and 0.36 mm^2 while maintaining sufficient accuracy for seizure detection in epileptic patients.**

***Index Terms*—Feature extraction, oscillatory synchronization, phase locking value (PLV), phase-amplitude coupling (PAC).**

I. Introduction

NEUROMODULATION is a promising therapy for neurological disorders such as epilepsy, treatment-resistant depression, and Parkinson's disease (PD) [1], [2], [3], [4]. Symptoms associated with these disorders arise from abnormal hyper- or hypo-synchronization across brain networks. Neuromodulation aims at restoring healthy synchronization by stimulating or inhibiting neural activity. Neural recordings can capture oscillatory synchronization features to perform precise closed-loop neuromodulation. Phase locking value (PLV) and phase-amplitude coupling (PAC) are commonly used features to quantify oscillatory synchronization. The features can be directly used to drive the neural stimulator [5], [6] or as inputs to the neural signal classifier driving the stimulation [7], [8], [9], [10].

The first step to calculate PLV and PAC is to divide the raw data into different frequency bands and obtain the complex representation for each band. Typically, this is achieved using Morlet wavelet convolutions [11], or a bandpass filter bank followed by Hilbert transforms [6], [7]. The Morlet wavelet extracts the real and imaginary parts for each band using two wavelet filters with the same magnitude response and a 90° phase shift. Morlet wavelet convolutions are rarely used for on-chip feature extraction because of their hardware complexity (e.g., 170 multipliers and 340 taps for the [6:10] Hz theta band assuming a 1024 Hz sampling rate). Instead, a filter bank can perform the band selection while a Hilbert transform extracts the imaginary parts of each band. Since the Hilbert transform is an all-pass filter with a 90° phase shift, it can be shared between several bands, making this approach more hardware-friendly. However, the required taps and multipliers are still significant (e.g., 37 multipliers and 75 taps for the theta band assuming a 1024 Hz sampling rate). Resource sharing can reduce the area and power consumption of the filter bank [6], [7]. However, this still requires memory for storing different coefficients for each band.

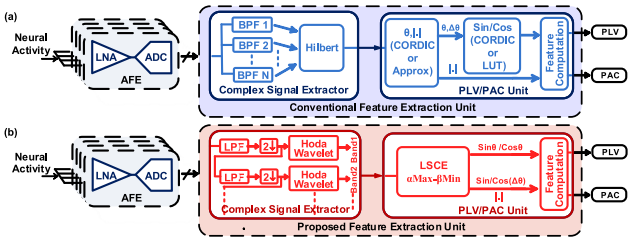

Fig. 1. System diagram of (a) a conventional feature extraction unit and (b) the proposed feature extraction unit.

The next step to calculate PLV and PAC is to extract the phase and magnitude from the complex signals - see Fig. 1(a). CORDIC processors perform accurate extraction at the cost of power and area efficiency [5]. To reduce the hardware complexity, a light phase extractor was proposed to approximate the phase while the amplitude is extracted using the l_∞-norm approximation [6]. However, trigonometric lookup tables (LUTs) are still required to implement the sine and cosine functions needed for calculating PAC and PLV. Coarse approximation methods have been proposed to calculate PLV directly without extracting any phase information [12], [13]. However, these methods suffer from lower accuracy and cannot extract PAC.

This brief expands upon our previous work by introducing a new complex signal extractor and combining it with the PLV/PAC unit proposed in [14] to construct a low-power oscillatory synchronization feature extraction unit - see Fig. 1(b). A new power-efficient multiplier-less wavelet approximation (the Hoda wavelet) is proposed and combined with a multi-rate lowpass filter (LPF) bank for complex signal extraction. The multi-rate operation reduces the total number of taps and eliminates the need for storing different coefficients for each band. The magnitude for the PLV/PAC unit is extracted using the more accurate αMax-βMin approximation. Also, a light

Manuscript received 15 August 2023; revised 16 November 2023 and 22 December 2023; accepted 10 January 2024. Date of publication 15 January 2024; date of current version 18 June 2024. This work was supported in part by the European Union's Horizon Europe Research and Innovation Programme under Grant 101070931, and in part by the Dutch Research Council under Grant 024.005.022. This brief was recommended by Associate Editor K.-H. Kim. *(Corresponding author: Hoda Yassin.)*

Hoda Yassin and El-Sayed Hasaneen are with the Department of Electrical Engineering, Aswan University, Aswan, Egypt (e-mail: HodaYassin@eng.aswu.edu.eg).

Arash Akhoundi and Dante G. Muratore are with the Department of Microelectronics, Delft University of Technology, 2600 AA Delft, The Netherlands.

Color versions of one or more figures in this article are available at https://doi.org/10.1109/TCSII.2024.3353927.

Digital Object Identifier 10.1109/TCSII.2024.3353927

sine and cosine extractor (LSCE) approximates the sine and cosine of the phase (or phase difference) directly from the complex signals, avoiding the complexity of phase extraction and trigonometric LUTs [14]. Section II explains the proposed complex signal extractor. The PLV/PAC unit is described in Section III. Simulation results are presented in Section IV, and conclusions are drawn in Section V.

II. Complex Signals Extractor Architecture

The first step in computing the synchronization features is to extract the complex signals within the observation frequency bands. Here we propose the Hoda wavelet and associate it with a multi-rate LPF bank as a complex signal extractor. The multiplier-less nature of the Hoda wavelet as well as the multi-rate operation of the LPF bank reduces the hardware complexity, and the area and power consumption.

A. The Hoda Wavelet

The Morlet wavelet is composed of sine and cosine functions multiplied by a Gaussian window which results in two bandpass filters with the same magnitude response and a 90° phase shift (Fig. 2(a)). The proposed Hoda wavelet replaces the sine and cosine with two square functions with a 90° phase shift. The square functions are multiplied by a four-level quantized window (Fig. 2(b)). The four levels are chosen to be [1, 0.75, 0.5, 0.25] and can be implemented using only bit shifters, avoiding the need for multipliers and a coefficient memory. Similar to the Morlet wavelet, the Hoda wavelet results in two bandpass filters with a 90° phase difference. The bandpass response shows side lobes at the odd harmonics of the center frequency due to the fast transitions in the time domain. The proposed Hoda wavelet can be seen as an extension of the Haar wavelet, which is composed of square-shaped functions multiplied by a rectangular window. The Hoda wavelet differs from the Haar wavelet by (1) being a complex-valued wavelet with both real and imaginary components, meaning it captures both amplitude and phase information of signals, and (2) having a 4-level window instead of a rectangular window which results in attenuation of the side lobes.

The center frequency (F_c) of the Hoda wavelet is the same as the frequency of the square waves, while the width of the multiplication window determines its bandwidth (BW), which can be approximated by:

$$BW = \frac{F_c}{N_{cyc}} \tag{1}$$

where N_{cyc} is the number of square wave cycles per wavelet. The quality factor of the Hoda wavelet ($Q = \frac{F_c}{BW}$) is equal to N_{cyc}. For a wavelet to capture both positive and negative components of signals equally, the mean value must be zero; and to perform complex signal extraction, the wavelet must be symmetric. For the Hoda wavelet to satisfy the zero mean and the symmetry properties, the number of the wavelet taps is recommended to be a multiplier of 8, while the N_{cyc} should be an even number with a minimum value of 2. Hence, for an input signal sampled at frequency F_s, the number of required taps (N_{wvlt}) to implement a wavelet is given by:

$$N_{wvlt} = N_{cyc}\frac{F_s}{F_c} \tag{2}$$

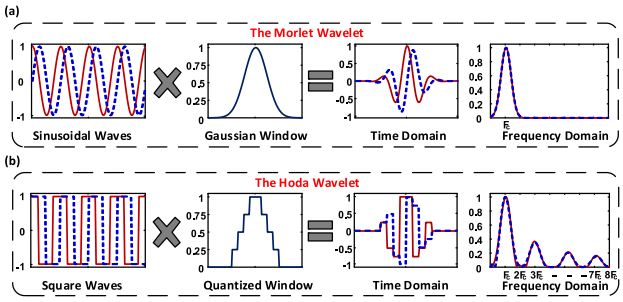

Fig. 2. The composition of (a) the Morlet wavelet and (b) the Hoda Wavelet.

The number of taps is inversely proportional to the wavelet center frequency. To prevent a large N_{wvlt} for low center frequencies, we propose to use decimation before each wavelet to fix the ratio between F_s and F_c. Decimation results in spectrum folding that can be limited using a LPF before decimation to avoid signal degradation. This LPF can also attenuate the unwanted high-frequency components captured by the wavelet side lobes. Typically, this application considers 8 to 10 effective number of bits (ENOB). Hence, the required stopband attenuation of the LPF is 62 dB to 50 dB. The stopband frequency (F_{stop}) and the transition band (ΔF) of the required LPF can be approximated as:

$$F_{Stop} = \frac{Fs}{DF} - 2.5Fc \tag{3}$$

$$\Delta F = \frac{Fs}{DF}\left(1 - \frac{7N_{cyc}+1}{2N_{wvlt}}\right) \tag{4}$$

$$DF = \frac{F_s N_{cyc}}{N_{wvlt} F_c} \tag{5}$$

where DF is the required decimation factor. A trade-off between the wavelet number of taps and the LPF complexity exists. To choose the optimal design point, N_{wvlt} is compared against the ratio of the sampling frequency to the transition band of the LPF as a proxy for its complexity (Fig. 3(a)). Here, the optimal value of N_{wvlt} is 16 taps. The chosen quality factor is $N_{cyc} = 2$, which is in the typical range for neural signals (based on the conventional delta, theta, alpha, beta, and gamma bands [7]). The time and frequency response of the wavelet family is shown in Fig. 3(b).

B. The LPF Design

Finite impulse response (FIR) filters have a linear phase response and are preferred to infinite impulse response (IIR) filters when extracting synchronization features. Specifically, the filter can be implemented as a conventional FIR lowpass filter or a cascaded integrator-comb filter (CIC). The conventional FIR filter has a flatter magnitude response at the cost of more taps, while the CIC has a sinc magnitude response but requires fewer taps. However, both filters have similar phase performance, which is the primary feature in synchronization features. Hence, this brief uses the CIC filter to reduce the system complexity and power consumption.

CIC filters can be implemented either by recursive or non-recursive structures. Recursive CIC (R-CIC) filters are implemented using only comb stages and integrators. The comb stage subtracts a delayed input sample from the current one, while the integrator works as an accumulator. Hence,

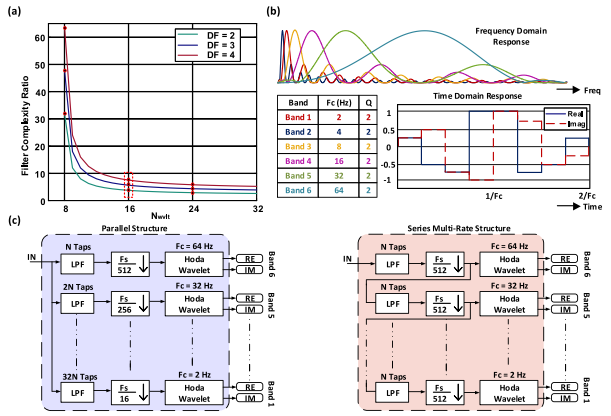

Fig. 3. The complex signal extractor design. (a) Filter complexity ratio as a function of N_{wvlt}. (b) The time and frequency responses of the utilized Hoda wavelet family. (c) Parallel and serial filter bank structures.

this structure does not require multipliers or a filter coefficient memory. However, the required arithmetic precision grows exponentially with the filter order, which is proportional to the desired decimation factor. This makes the register bit width unacceptably large (e.g., 18-bit registers for an 8^{th}-order CIC filter considering $2\times$ DF and 10-bit input width). Alternatively, non-recursive CIC (NR-CIC) filters are implemented similarly to FIR filters using multipliers and adders but with fewer taps. The number of taps for an NR-CIC filter (N_{NR-CIC}) is proportional to the required decimation factor.

Furthermore, either filter bank can be implemented using a parallel or series structure (Fig. 3(c)). The desired decimation factor after each LPF in the filter bank is inversely proportional to the wavelet center frequency. Hence, the parallel structure suffers from an exponential increment in the LPF taps for low center frequencies. The series multi-rate structure solves this issue at the cost of increasing the delay mismatch between the different bands. This delay is undesired for the PAC and it has to be compensated (more details in Section III). Considering an input sampling frequency of 1024 Hz and the designed wavelet family, the decimation factor after each filter (DF_s) is 2 for the series implementation.

All possible filter implementations are compared and summarized in Table I. Here, the filter bank is implemented using the series multi-rate structure, and the LPF is designed as an 8^{th}-order NR-CIC filter (highlighted in the table).

TABLE I
SUMMARY OF THE LPF IMPLEMENTATIONS COMPARISON

Structure			No LPF	Parallel			Series (Multi-Rate)		
				FIR	R-CIC	NR-CIC	FIR	R-CIC	NR-CIC
No. Taps	LPF	F1	-	15	16	9	15	16	9
		F2	-	30		17			
		:	-	:		:			
		F6	-	480		257			
	Wavelet	W1	32	16			16		
		W2	64						
		:	:						
		W6	1024						
LPF Registers (bits)		F1	-	10	18	10	10	18	10
		F2	-		26				
		:	-		:				
		F6	-		58				
LPF Multipliers			-	Y	N	Y	Y	N	Y
LPF Mag (dB)			-	0.2	1.5	1.5	0.2	1.5	1.5
Delay of Band (ms)		1	15	21	26	18.5	21.5	26	18.5
		2	31	43	49	22.5	50	64	41
		:	:	:	:	:	:	:	:
		6	500	702	722	594	1000	1200	741
ENOB (bits)			8 : 9						

III. PLV/PAC ARCHITECTURE

Phase locking value (PLV) and phase-amplitude coupling (PAC) are two commonly used features to quantify oscillatory synchronization. PLV measures the level of phase synchronization between two intra-band neural signals S_1 and S_2 as:

$$PLV = \frac{1}{N}\sqrt{\left(\sum_{i=1}^{N} sin\Delta\theta_i\right)^2 + \left(\sum_{i=1}^{N} cos\Delta\theta_i\right)^2} \quad (6)$$

$$\Delta\theta_i = \theta_{2,i} - \theta_{1,i} \quad (7)$$

where N is the number of samples of the averaging time window, and $\theta_{1,i}$ and $\theta_{2,i}$ are the instantaneous phases of S_1 and S_2 at the i^{th} sample.

PAC is a cross-frequency feature in which the phase of a low-frequency oscillation modulates the amplitude of a high-frequency oscillation. PAC is widely measured as:

$$PAC = \frac{1}{N}\sqrt{\left(\sum_{i=1}^{N} A_{m,i}sin\theta_{p,i}\right)^2 + \left(\sum_{i=1}^{N} A_{m,i}cos\theta_{p,i}\right)^2} \quad (8)$$

where N is the number of samples of the averaging time window, $\theta_{p,i}$ is the instantaneous phase of the low-frequency phase-modulating signal, and $A_{m,i}$ is the instantaneous magnitude of the high-frequency amplitude-modulated signal, at the i^{th} sample.

The PLV/PAC unit receives decimated signals from the complex signal extractor; however, this does not affect the minimum feature window length as it is still limited by the lowest frequency in the band of interest. Notably, extremely short windows compromise feature accuracy, while long windows increase latency [15]. Thus, there is a general accuracy-latency trade-off to consider. Our implementation strikes a balance, utilizing window sizes comparable to conventional literature (e.g., 2 s in [16]).

The block diagram of the proposed PLV/PAC unit is shown in Fig. 4(a). First, the real and imaginary parts of the PLV input signals (RE_1, IM_1, RE_2, IM_2) are applied to a $\Delta\theta$ extractor to generate a new complex signal with a phase equal to the phase difference between the two input signals. Then, the output of the $\Delta\theta$ extractor ($RE_{\Delta\theta}$, $IM_{\Delta\theta}$) as well as the real and imaginary parts of the PAC phase-modulating signal (RE_p, IM_p) are applied to a shared LSCE to get $\sin\Delta\theta/\cos\Delta\theta$ for PLV and $\sin\theta_p/\cos\theta_p$ for PAC. Also, the real and imaginary parts of the PAC amplitude-modulated signal (RE_A, IM_A) are applied to a magnitude extraction module. The output of the PAC magnitude extractor is applied to a delay compensation module to compensate for the delay and sampling rate mismatch between the PAC phase-modulating signal and amplitude-modulated signal, introduced by the multi-rate LPF in Section II. Shared accumulators and shifters are used to perform the averaging over a predefined time window. Finally, a magnitude extraction module is utilized to get the final values of PLV and PAC. Each sub-block is described in detail below.

A. $\Delta\theta$ Extractor

Since the proposed method never extracts the phase of the input signals, the PLV inputs have to be combined to generate a new complex signal with a phase equal to $\Delta\theta$ to feed to the LSCE. For two input signals S_1 and S_2 with phases θ_1

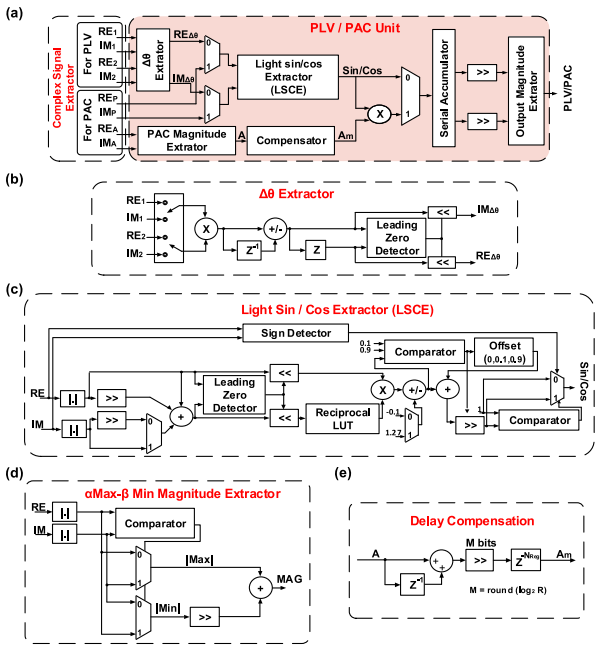

Fig. 4. (a) The PLV/PAC unit block diagram. (b) The $\Delta\theta$ extractor block diagram. (c) The LSCE block diagram. (d) The αMax-βMin magnitude extractor block diagram. (e) The delay compensation block diagram.

and θ_2, the real and imaginary parts of a signal with phase $\Delta\theta = \theta_2 - \theta_1$ are given as:

$$RE_{\Delta\theta} = RE_1 \times RE_2 + IM_1 \times IM_2 \quad (9)$$

$$IM_{\Delta\theta} = IM_2 \times RE_1 - IM_1 \times RE_2 \quad (10)$$

where RE_1, IM_1 and RE_2, IM_2 are the real and imaginary parts of S_1 and S_2, respectively.

$\Delta\theta$ Extractor is implemented with one multiplier and one adder running at 4× the input rate. A leading zero detector and shifters are used to detect small outputs and multiply them by a constant to reduce truncation errors (Fig. 4(b)).

B. Light Sine and Cosine Extractor

The LSCE approximates the sine and cosine of phases directly from complex signals. To do so, the sine and cosine are plotted as functions of the real-to-imaginary components ratio. The resultant curves are divided into four intervals, and curve fitting is performed for each interval to obtain the approximation formulas (Fig. 5). Using more curve-fitting intervals results in higher accuracy at the cost of complexity and vice versa. To address this trade-off, we chose the number of intervals that achieve sufficient accuracy for computing PLV/PAC with low complexity. The similarity between the sine and cosine approximation formulas makes it possible to share resources and implement a single sin/cos extraction unit (Fig. 4(c).

C. αMax-βMin Magnitude Extractor

The αMax-βMin algorithm approximates the magnitude as $A = 0.945(|Max| + 0.5|Min|)$, where $|Max|$ and $|Min|$ are the maximum and the minimum between the absolute values of the real and the imaginary parts, respectively (Fig. 4(d)). The factor 0.945 is omitted as it does not introduce any necessary information for the PAC/PLV extraction. The error introduced

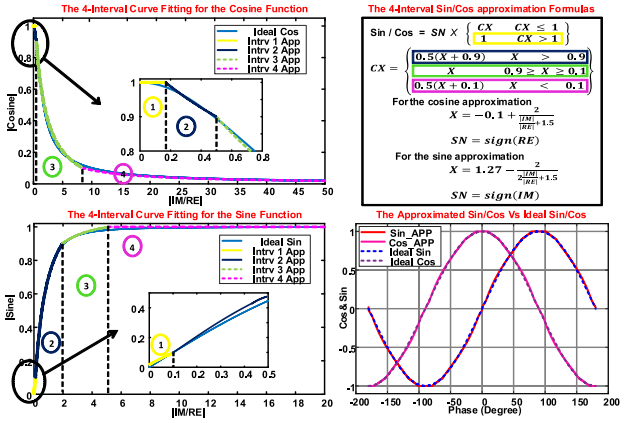

Fig. 5. Approximated sine and cosine functions for the LSCE unit.

by the αMax-βMin approximation appears as a high-frequency ripple with a maximum percentage error of ± 5.5%. This error does not affect the intra-band PAC state, and its effect on the output magnitude accuracy is negligible [14].

D. Delay Compensation

The multi-rate operation of the complex signal extractor results in delay and data rate mismatches between the different bands. High-frequency bands have higher data rates, while low-frequency bands have longer delays. These mismatches are undesired for the PAC, and a delay compensation module is needed. First, the data rate mismatch is compensated by averaging the PAC extracted magnitude over R samples, where R is the ratio of the sampling rate of the PAC amplitude-modulated band to the sampling rate of the PAC phase-modulating band. Then, the averaged magnitude is applied to a chain of registers to compensate for the delay mismatch (Fig. 4(e)). The number of the required delay registers is:

$$N_{Reg} = (N_{wvlt} - 1)\frac{R-1}{2R} + \frac{N_{LPF}-1}{2R}\sum_{n=1}^{\log_{DF_s}(R)-1} DF_s^n \quad (11)$$

where N_{LPF} is the number of taps required by the complex signal extractor LPF. Here, the worst mismatch exists between Band1 and Band6, where $N_{Reg} = 11$ and $R = 32$.

IV. Simulation Results

A MATLAB hardware model of the feature extraction unit is validated using the CHB-MIT scalp EEG database [17]. This database is collected at the Children's Hospital Boston from pediatric subjects with intractable epileptic seizures using the international 10-20 EEG electrode positions and a sampling rate of 256 Hz with 16-bit resolution. The data is quantized to 10 bits and interpolated to a rate of 1024 Hz before the feature extraction unit. Band2 ([3:5] Hz, a sub-band of theta) is chosen as the PLV extraction band as well as the phase-modulating band for PAC. The amplitude-modulated band for PAC is set to Band6 ([48:80] Hz, a sub-band of gamma).

A useful feature exhibits a significant variation during the event of interest, which makes the classification easier. To validate the performance of the proposed extractor, the peak-to-average ratio (PAPR) is calculated for each seizure event and compared to the ideal features extracted using the Morlet

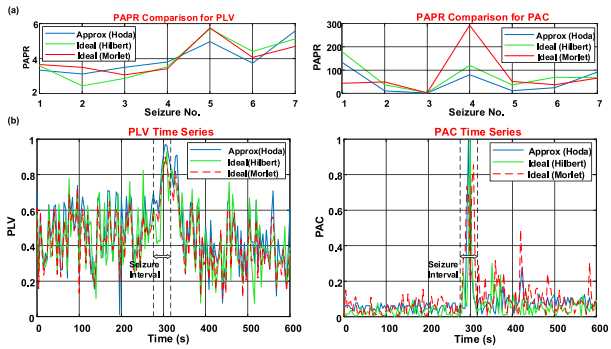

Fig. 6. Simulation results of the feature extraction unit. (a) PAPR comparison across all seizure events for Patient No.1. For each PAPR, the peak value is the maximum feature power within the seizure interval, while the average power is computed at a non-seizure interval over a time window that is 6× the seizure interval. The time window is divided equally before and after the seizure. (b) Time series comparison of the extracted features using a 4-second time window over a 600-second time interval with a 32-second seizure event.

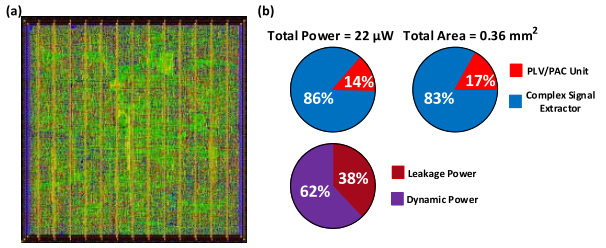

Fig. 7. The proposed FE unit (a) layout view and (b) power/area breakdown.

and Hilbert methods, showing a competitive performance (Fig. 6(a)). Furthermore, the proposed method achieves a cosine similarity of 99% for PLV and 92.5% for PAC when compared to Morlet method, and 98.7% for PLV and 97% for PAC when compared to Hilbert method. This is close to the similarity between Morlet and Hilbet methods (99.1% for PLV, and 94.3% for PAC). For illustration purposes, the time series of the compared features are plotted over a 600-second interval with a 32-second seizure event (Fig. 6(b)). In summary, the extracted features approximate the ideal features closely, showing their suitability for seizure detection.

A 32-channel HDL implementation of the proposed feature extraction was synthesized in 40-nm CMOS technology. The design receives the output of 64 recording channels and comprises two complex signal extractors processing 32 channels each and running at 32 kHz, and a single PLV/PAC unit that processes the decimated output of the complex signal extractor. The design consumes a total power of 22 μW and occupies a core area of 0.36 mm^2 based on post-layout simulations (Fig. 7). A comparison between the simulation results of the proposed feature extraction unit and the state of the art is given in Table II. This brief achieves the best area and power performance per channel over the feature extraction units.

V. Conclusion

This brief presents a low-power feature extraction unit for the PAC and PLV features. A new multiplier-less wavelet approximation is proposed and combined with a multi-rate LPF bank to extract the required complex signal. Power and area consumption is further reduced by using a LSCE for the feature computation. The proposed design achieves 688 nW/channel and 0.011 mm^2/channel while maintaining sufficient accuracy for epileptic seizure detection.

TABLE II
Comparison With the State-of-the-Art

Parameter	JSSC'13 [5]	JSSC'18 [7]	CICC'22 [6]	This Work
Process (nm)	130	130	65	40
Supply Voltage (V)	1.2	1.2	0.85	1.1
PLV/PAC channels	32 PLV	64 PAC/PLV^d	8 PAC/PLV	32 PAC/PLV
Area (mm^2)	0.959^a	0.97^b	0.387^a	0.36^c
Area/ch (mm^2)	0.03	0.015	0.048	0.011
Total Power (μW)	656	225^e	14.4	22
Power/ch (μW)	20.5	3.5	1.8	0.688

^{a}Estimated from reported total area and the percentage area occupied by the FE unit.
^{b}Estimated from reported total area and the SoC micrograph.
^{c}Reported after place and route. ^{d}Estimated # of extracted features. ^{e}Without digital filters and memory.

References

[1] R. Fisher et al., "Electrical stimulation of the anterior nucleus of thalamus for treatment of refractory epilepsy," *Epilepsia*, vol. 51, no. 5, pp. 899–908, May 2010.
[2] M. Pais-Vieira et al., "A closed loop brain-machine interface for epilepsy control using dorsal column electrical stimulation," *Sci. Rep.*, vol. 6, no. 1, 2016, Art. no. 32814.
[3] K. W. Scangos et al., "Closed-loop neuromodulation in an individual with treatment-resistant depression," *Nature Med.*, vol. 27, no. 10, pp. 1696–1700, 2021.
[4] C. R. Sullivan, S. Olsen, and A. S. Widge, "Deep brain stimulation for psychiatric disorders: From focal brain targets to cognitive networks," *Neuroimage*, vol. 225, Jan. 2021, Art. no. 117515.
[5] K. Abdelhalim, H. M. Jafari, L. Kokarovtseva, J. L. P. Velazquez, and R. Genov, "64-channel UWB wireless neural vector Analyzer SOC with a closed-loop phase synchrony-triggered neurostimulator," *IEEE J. Solid-State Circuits*, vol. 48, no. 10, pp. 2494–2510, Oct. 2013.
[6] U. Shin, C. Ding, L. Somappa, V. Woods, A. S. Widge, and M. Shoaran, "A 16-channel 60μW neural synchrony processor for multi-mode phase-locked neurostimulation," in *Proc. IEEE Custom Integr. Circuits Conf. (CICC)*, 2022, pp. 1–2.
[7] G. O'Leary, D. M. Groppe, T. A. Valiante, N. Verma, and R. Genov, "NURIP: Neural interface processor for brain-state classification and programmable-waveform neurostimulation," *IEEE J. Solid-State Circuits*, vol. 53, no. 11, pp. 3150–3162, Nov. 2018.
[8] C.-H. Cheng et al., "A fully integrated 16-channel closed-loop neural-prosthetic CMOS SoC with wireless power and bidirectional data telemetry for real-time efficient human epileptic seizure control," *IEEE J. Solid-State Circuits*, vol. 53, no. 11, pp. 3314–3326, Nov. 2018.
[9] L. Yao, P. Brown, and M. Shoaran, "Resting tremor detection in parkinson's disease with machine learning and Kalman filtering," in *Proc. IEEE Biomed. Circuits Syst. Conf.*, 2019, pp. 1–4.
[10] M. Zhang et al., "A one-shot learning, online-tuning, closed-loop epilepsy management SoC with 0.97μJ/classification and 97% vector-based sensitivity," in *Proc. Symp. VLSI Circuits*, 2021, pp. 1–2.
[11] S. Morales and M. E. Bowers, "Time-frequency analysis methods and their application in developmental EEG data," *Develop. Cogn. Neurosci.*, vol. 54, Apr. 2022, Art. no. 101067.
[12] S. Dávila-Montero and A. J. Mason, "An in-situ phase-preserving data decimation method for high-channel-count wireless μECoG arrays," in *Proc. IEEE Biomed. Circuits Syst. Conf. (BioCAS)*, 2017, pp. 1–4.
[13] M. Delgado-Restituto, J. B. Romaine, and A. Rodriguez-Vazquez, "Phase synchronization operator for on-chip brain functional connectivity computation," *IEEE Trans. Biomed. Circuits Syst.*, vol. 13, no. 5, pp. 957–970, Oct. 2019.
[14] H. Yassin, A. Akhoundi, E.-S. Hasaneen, and D. G. Muratore, "A low-power oscillatory feature extraction unit for Implantable neural interfaces," in *Proc. IEEE Int. Symp. Circuits Syst. (ISCAS)*, 2023, pp. 1–5.
[15] K. Abdelhalim, V. Smolyakov, and R. Genov, "Phase-synchronization early epileptic seizure detector VLSI architecture," *IEEE Trans. Biomed. Circuits Syst.*, vol. 5, no. 5, pp. 430–438, Oct. 2011.
[16] C. Fan, B. Yang, X. Li, and P. Zan, "Temporal-frequency-phase feature classification using 3D-convolutional neural networks for motor imagery and movement," *Front. Neurosci.*, vol. 17, Aug. 2023, Art. no. 1250991.
[17] A. H. Shoeb, "Application of machine learning to epileptic seizure onset detection and treatment," Ph.D. dissertation, Massachusetts Inst. Technol., Cambridge, MA, USA, 2009.